JGR Oceans

RESEARCH ARTICLE
10.1029/2022JC019113

Generation of the Internal Pycnocline in the Subpolar Southern Ocean by Wintertime Sea Ice Melting

A. Klocker[1,2,3], A. C. Naveira Garabato[4], F. Roquet[5], C. de Lavergne[6], and S. R. Rintoul[7,8,9]

[1]Institute for Marine and Antarctic Studies, University of Tasmania, Hobart, TAS, Australia, [2]Australian Research Council Centre of Excellence for Climate Extremes, University of Tasmania, Hobart, TAS, Australia, [3]Now at NORCE Norwegian Research Centre, Bjerknes Centre for Climate Research, Bergen, Norway, [4]Ocean and Earth Science, National Oceanography Centre, University of Southampton, Southampton, UK, [5]Department of Marine Sciences, University of Gothenburg, Gothenburg, Sweden, [6]LOCEAN Laboratory, Sorbonne University-CNRS-IRD-MNHN, Paris, France, [7]Commonwealth Scientific and Industrial Research Organisation, Environment, Hobart, TAS, Australia, [8]Centre for Southern Hemisphere Oceans Research, CSIRO, Hobart, TAS, Australia, [9]Australian Antarctic Program Partnership, University of Tasmania, Hobart, TAS, Australia

Key Points:

- The internal pycnocline in the high-latitude Southern Ocean is generated by winter-persistent sea ice melting
- Sea-ice melt persists in winter due to ice drift and warm-water entrainment, thus maintaining salinity-based stratification at the base of the winter mixed layer
- The subpolar internal pycnocline descends into the ocean interior at fronts of the Antarctic Circumpolar Current

Correspondence to:
A. Klocker,
ankl@norceresearch.no

Citation:
Klocker, A., Naveira Garabato, A. C., Roquet, F., de Lavergne, C., & Rintoul, S. R. (2023). Generation of the internal pycnocline in the subpolar Southern Ocean by wintertime sea ice melting. *Journal of Geophysical Research: Oceans*, *128*, e2022JC019113. https://doi.org/10.1029/2022JC019113

Received 23 JUL 2022
Accepted 9 MAR 2023

The copyright line for this article was changed on 21 APR 2023 after original online publication.

Abstract The ocean's internal pycnocline is a layer of elevated stratification that separates the well-ventilated upper ocean from the more slowly renewed deep ocean. Despite its pivotal role in organizing ocean circulation, the processes governing the formation of the internal pycnocline remain little understood. Classical theories on pycnocline formation have been couched in terms of temperature and it is not clear how the theory applies in the high-latitude Southern Ocean, where stratification is dominated by salinity. Here we assess the mechanisms generating the internal pycnocline at southern high latitudes through the analysis of a high-resolution, realistic, global sea ice–ocean model. We show evidence suggesting that the internal pycnocline's formation is associated with sea ice-ocean interactions in two distinct ice-covered regions, fringing the Antarctic continental slope and the winter sea-ice edge. In both areas, winter-persistent sea-ice melt creates strong, salinity-based stratification at the base of the winter mixed layer. The resulting sheets of high stratification subsequently descend into the ocean interior at fronts of the Antarctic Circumpolar Current, and connect seamlessly to the internal pycnocline in areas further north in which pycnocline stratification is determined by temperature. Our findings thus suggest an important role of localized sea ice-ocean interactions in configuring the vertical structure of the Southern Ocean.

Plain Language Summary Satellite observations have revealed significant trends in Antarctic sea-ice concentration over recent decades. While the science community is starting to unravel the causes of the observed changes in sea-ice extent, our understanding of how these ice changes are influencing ocean circulation remains rudimentary. Here we take a step toward addressing this important gap by analyzing relationships between sea ice and ocean density structure in a state-of-the-art, realistic sea ice-ocean model. We find that localized sea ice-ocean interactions in the Southern Ocean, in particular the counter-intuitive melting of sea ice in winter, contribute to shape the vertical structure of the Southern Hemisphere oceans.

1. Introduction

The internal pycnocline is a perennial layer of elevated density stratification, found at 200–1,500 m over much of the ocean (Gnanadesikan, 1999; Samelson & Vallis, 1997). It is the main organizing feature of global ocean circulation, as it separates the relatively well-ventilated waters of the upper ocean, including those of the ventilated pycnocline (Luyten et al., 1983), from more slowly renewed deeper waters (DeVries & Primeau, 2011). The abrupt vertical gradient in renewal time scale associated with the internal pycnocline structures many important oceanic physical and chemical properties, such as salinity (Figures 1b, 1d, and 1f) or dissolved inorganic carbon (Talley et al., 2016), thus fundamentally shaping the ocean's climatic role (Khatiwala et al., 2012).

Classical views of the pycnocline—historically referred to as thermocline theory, since past work has focused on regions where stratification is set by temperature (often termed the *alpha ocean*, see (Carmack, 2007))—propose two distinct mechanisms of pycnocline formation. In adiabatic theories (Huang, 1988; Luyten et al., 1983; Welander, 1959), the surface density distribution is set by atmospheric thermal forcing and transferred to the ocean interior by wind-driven Ekman downwelling, which maps the surface meridional density gradient to a vertical profile. In contrast, diabatic theories (Robinson & Stommel, 1959; Salmon, 1990; Stommel & Webster, 1962;

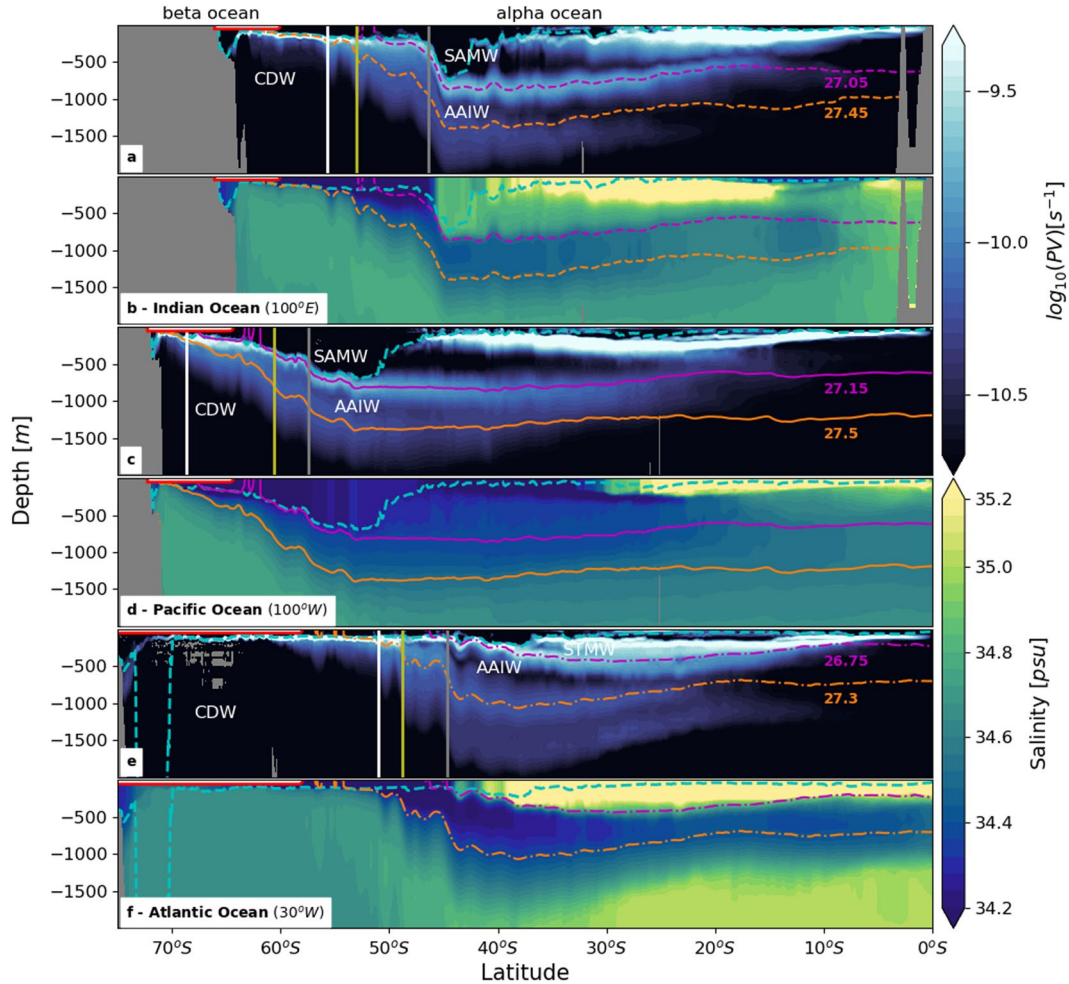

Figure 1. Potential vorticity and salinity. Winter values (shown for the month of September 2015) of (a, c, e) $\log_{10}$(|PV|) and (b, d, f) salinity for a representative section in (a), (b) the South Indian Ocean (100°E), (c), (d) the South Pacific Ocean (100°W) and (e), (f) the South Atlantic Ocean (30°W). Colored lines are isopycnal surfaces associated with the upper (magenta) and lower (orange) high-PV sheets, which together form the internal pycnocline.

Young & Ierley, 1986) interpret the pycnocline as a diffusive front (or internal boundary layer) that forms at the convergence of warm near-surface waters and upwelling cold abyssal waters. In this view, the pycnocline thickness decreases as diabatic mixing weakens. Such adiabatic and diabatic perspectives on pycnocline generation were subsequently unified in a two-regime model (Samelson & Vallis, 1997), according to which an upper, adiabatic part of the pycnocline (the ventilated pycnocline) results from the vertical mapping of the surface meridional temperature gradient across the subtropical gyre; and a lower, diabatic part of the pycnocline (the internal pycnocline) is generated via a vertical advection—diffusion balance, which recasts the surface meridional temperature difference across the subpolar gyre onto the vertical. This two-regime model, derived for a single-hemisphere closed basin, reproduces the main characteristics of the subtropical pycnocline and constitutes, to this day, the standard point of reference upon which our understanding of the pycnocline is based.

However, classical pycnocline theories may not directly address where or how extensive parts of the internal pycnocline, such as that pervading the Southern Ocean, are formed. In much of that region, stratification is primarily determined by salinity (a regime often termed the *beta ocean* (Carmack, 2007)), with temperature having a destabilizing effect on stratification. By focusing on temperature stratification, classical thermocline theories neglect potentially influential nonlinear interactions between temperature and salinity. Nonlinear interactions may arise in two main ways: (a) via the nonlinear dependence of density on temperature, salinity, and pressure; and (b) via the forcing of surface ocean temperature and salinity through distinct mechanisms with different spatio-temporal scales. Nowhere is the significance of such nonlinear interactions more evident than in the polar

regions. There, the dominance of salinity in determining upper-ocean stratification maintains vast volumes of warm waters below the pycnocline and favors the wintertime formation of sea ice (Carmack, 2007)—the presence of which creates a powerful coupling between heat and freshwater fluxes (Lecomte et al., 2017; Martinson, 1990; Polyakov et al., 2017; Wilson et al., 2019). Recent work demonstrates the prominent global stratification impact of the nonlinear dependence of density on temperature and pressure (Nycander et al., 2015; Roquet et al., 2015), and highlights the large sensitivity of global stratification and sea-ice formation to seawater properties near the freezing point (Roquet et al., 2022).

In this paper, we show evidence from a realistic sea ice-ocean model which suggests that nonlinear interactions between temperature and salinity play an important role in the generation of the internal pycnocline in the subpolar Southern Ocean. Our illustration of this result is framed in terms of potential vorticity (PV). Although vigorously modified at the ocean boundaries, PV is approximately conserved in the ocean interior, where diabatic and frictional processes are generally modest (Vallis, 2006). Here, we define $\mathrm{PV} = -\frac{f}{\rho}\frac{d\rho}{dz}$, where f is the Coriolis parameter, ρ is the surface-referenced potential density, and $\frac{1}{\rho}\frac{d\rho}{dz}$ quantifies the vertical stretching of isopycnal layers. Relative vorticity is neglected in this definition, as it is small relative to planetary vorticity except in localized frontal regions (J. Marshall et al., 1993). Thus, PV is closely related to stratification, and the internal pycnocline is found to comprise several two-dimensional surfaces along which PV is elevated. We will refer to these two-dimensional surfaces as *high-PV sheets*.

2. Data and Methods

2.1. Global Eddying Sea Ice-Ocean Model

Observations that resolve the seasonal cycle of surface forcing and hydrography in the Southern Ocean are presently scarce. We therefore turn to an eddying global sea ice-ocean simulation that has been thoroughly compared with observations and proven to be reasonably realistic (Kiss et al., 2020). The use of model output allows seasonally varying surface fluxes to be linked to the seasonal evolution of stratification and PV. This enables us, in turn, to build an integrated picture of processes leading to the structure of the internal pycnocline.

The simulation uses a mesoscale eddy-rich version of the sea ice-ocean implementation of the Australian Community Climate and Earth System Simulator, ACCESS-OM2, run at a horizontal resolution of 0.1° (ACCESS-OM2-01) with 75 vertical levels. The ocean model is MOM5.1 and the sea-ice model CICE5.1, coupled with the OASIS-MCT coupler. The model was forced with the JRA55-do v1.3 forcing data set. The ACCESS-OM2-01 experiment ran for 33 years from 1 January 1985 to 31 December 2017. It was started from a 40-year spin-up under repeated 1 May 1984–30 April 1985 JRA55-do forcing. Note that, while below we define the Stratification Control Index (SCI; see Appendix B for further detail) in terms of conservative temperature Θ and absolute salinity S_A, the model uses potential temperature θ and practical salinity S_P instead. Hence, both PV and the SCI in the model are calculated using θ and S_P. Model fields are available as monthly means. Details of the simulation and its evaluation can be found elsewhere (Kiss et al., 2020).

2.2. One-Dimensional Model of Pycnocline Generation

To understand the separate roles of temperature, salinity and wind forcing in the generation of the subpolar Southern Ocean pycnocline, we use the Massachusetts Institute of Technology general circulation model (MITgcm (J. Marshall et al., 1997)) in a simple one-dimensional configuration with boundary conditions taken from the eddying global sea ice-ocean simulation. The 1-d model domain spans the uppermost 500 m of the water column, and has a vertical resolution of 1 m. Vertical mixing is parameterized using the K-profile parameterization (KPP (Large et al., 1994)). At the ocean surface and at 500 m, the 1-d model is restored to monthly mean temperature and salinity values with a restoring time scale of 1 day, and a monthly mean wind stress is applied at the surface. These values are taken from two locations in the global simulation (70°S, 100°W and 65°S, 100°W), which are sited along the Pacific transect shown in Figures 1c and 1d. The 1-d model is initialized with conditions for December 2014, and cycled through 1 year of boundary conditions. The 1-d model simulations are spun up for 200 years, and the last 3 years are considered for analysis. In each of the two locations, we run (a) a simulation with temperature/salinity/wind forcing, (b) a simulation in which we exclude temperature forcing, (c) a simulation in which we exclude salinity forcing, and (d) a simulation without wind forcing. Intercomparison of

these simulations enables us to highlight the crucial role of salinity forcing, set largely by sea ice-ocean interactions, in the generation of the local pycnocline.

3. Results and Discussion

3.1. Relating Potential Vorticity to the Southern Hemisphere's Ocean Structure

The distribution of PV provides the organizing framework for the large-scale water mass structure and vertical circulation of the ocean. In the Southern Ocean and neighboring Southern Hemisphere basins, this may be readily illustrated with meridional sections of PV across the Indian, Pacific, and Atlantic sectors (Figure 1). PV exhibits a layered arrangement, whereby thick layers of low PV are separated by thinner sheets of high PV. The thick, low-PV layers correspond to the major oceanic water masses, which feature prominently in syntheses of the Southern Hemisphere ocean circulation (Talley, 2013; A. C. Naveira Garabato et al., 2014).

Subantarctic Mode Water (SAMW), Antarctic Intermediate Water (AAIW), Circumpolar Deep Water (CDW) and Subtropical Mode Water (STMW) are labeled. The dashed cyan line represents the mixed layer depth. Vertical lines mark Southern Ocean fronts, in particular the Southern ACC front (SACCF; white), the Polar Front (PF; olive), and the Subantarctic Front (SAF; gray). Fronts are identified by maxima in isopycnal slopes and zonal flow, together with visual inspection of relevant hydrographic property gradients (Orsi et al., 1995). The red line at the surface shows the sea-ice extent, defined by sea-ice concentrations in excess of 15%. The beta ocean, in which stratification is determined by salinity, lies south of the PF. The alpha ocean, in which stratification is determined by temperature, lies north of the SAF.

Specifically, the low-PV layers extending northward from the Southern Ocean in both the Indian and Pacific basins at depths of <800 m contain Subantarctic Mode Water (SAMW; Figures 1a–1d). In the Atlantic basin, a low-PV layer residing at depths of <500 m encompasses Subtropical Mode Water (STMW; Figures 1e and 1f). The low-PV layers extending northward from the Southern Ocean in the Indian and Pacific basins (Atlantic basin) at depths of ∼1,000 m (∼700 m) contain Antarctic Intermediate Water (AAIW). AAIW exhibits a broad sub-surface salinity minimum (Figures 1b, 1d, and 1f). Both STMW/SAMW, and AAIW are characterized by relatively short ventilation time scales (DeVries & Primeau, 2011; McCartney, 1977). The deepest low-PV layer visible in Figure 1 encompasses Circumpolar Deep Water (CDW), a voluminous, slowly renewed water mass that has sources in the North Atlantic and ultimately upwells in the Southern Ocean (Tamsitt et al., 2017). All of these water masses acquire their low PV at their surface formation sites, where intense wind and buoyancy forcings in winter trigger convective mixing and destroy stratification (Bullister et al., 2001; Speer & Forget, 2001).

In turn, the high-PV sheets bounding the low-PV layers define the fabric of the ocean's pycnocline. The high-PV sheet closely following the 27.15 kg m^{-3} (27.05 kg m^{-3}) isopycnal in the Pacific (Indian) basin embodies the SAMW-AAIW interface. A less pronounced high-PV sheet is found at higher density, following the 27.5 kg m^{-3} (27.45 kg m^{-3}) isopycnal in the Pacific (Indian) Ocean, and constitutes the AAIW-CDW interface. A similar framework of two high-PV sheets exists in the Atlantic basin, where the sheets follow lighter isopycnals than in the Indo-Pacific sector and act as the STMW-AAIW and AAIW-CDW interfaces.

Jointly, the two high-PV sheets in the Pacific and Indian basins, at the upper and lower boundaries of AAIW, give rise to the stratification maximum that defines the internal pycnocline (In Figures 1a–1d, the internal pycnocline is the region of elevated PV between the magenta and orange density contours.) In the Atlantic basin, the internal pycnocline integrates only the denser high-PV sheet (the lighter sheet is embedded within the subtropical gyre's base, and thereby contributes to the ventilated pycnocline). In all basins, the internal pycnocline extends seamlessly from mid latitudes, across the Southern Ocean, to the Antarctic margins. The simulated pycnocline structure resembles that identified in hydrographic observations (Figure A1; Appendix A), although the observations display a more subtle inter-sheet separation concealed by finescale processes (such as internal waves) absent from the model, and slight differences in the density of the high-PV sheets. A possible factor underpinning the model-observations differences is the model's use of zero explicit background vertical diffusion. Although this is unlikely the most realistic choice, zero background diffusion facilitates the tracing of the Southern Ocean pycnocline's PV signature to its generation regions, and thereby results in a clearer view of the generation mechanism.

The anatomy of the high-PV sheets forming the internal pycnocline offers several important hints as to the pycnocline's origin (Figures 1a, 1c, and 1e). As one traces the high-PV sheets southward, approximately following

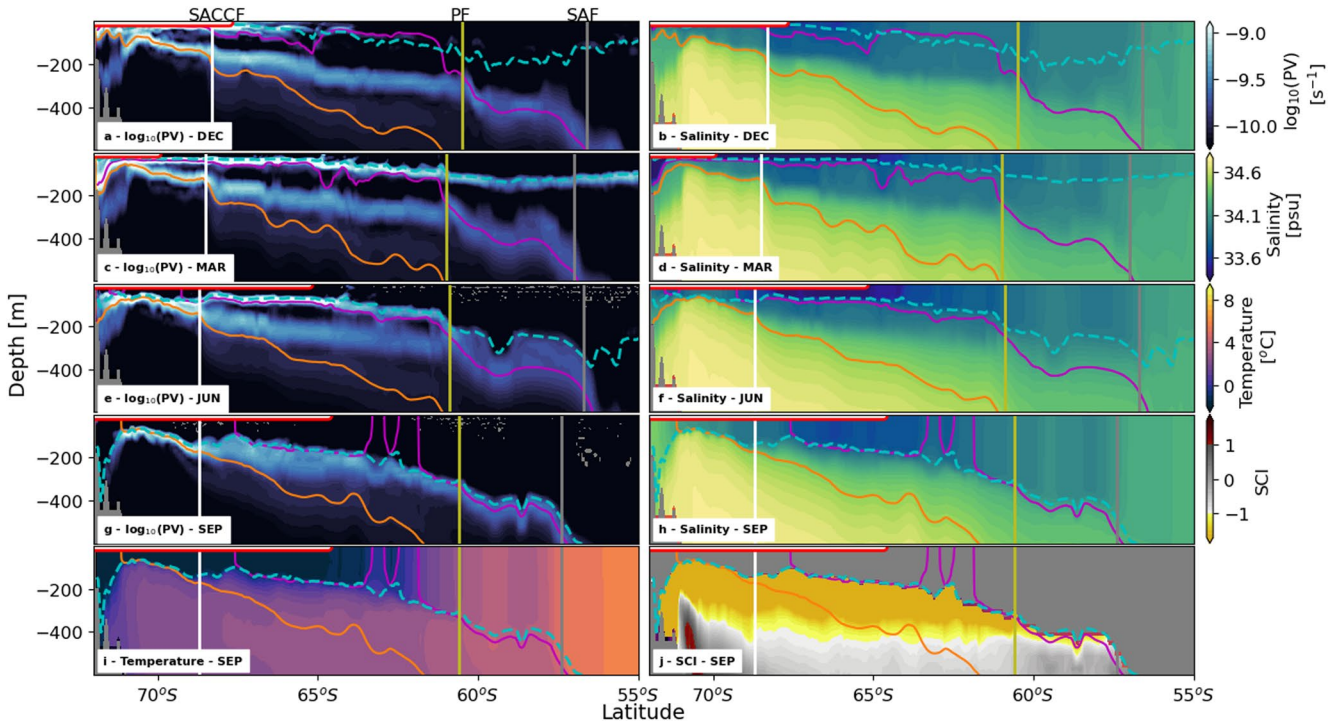

Figure 2. Seasonal evolution of potential vorticity and salinity in the Pacific sector. A latitude-depth section at 100°W of (a, c, e, g) $\log_{10}(|PV|)$ and (b, d, f, h) salinity for (a), (b) December, (c), (d) March, (e), (f) June, and (g), (h) September of year 2014/2015. (i) Temperature, and (j) Stratification Control Index SCI at 100°W for June 2015. Colored lines are isopycnal surfaces $\sigma_\Theta = 27.15$ kg m^{-3} (magenta) and 27.5 kg m^{-3} (orange). Dashed cyan line shows the mixed layer depth. Vertical lines mark Southern Ocean fronts, in particular, the Southern ACC front (white), the Polar Front (PF; olive) and the Subantarctic Front (gray). Fronts are identified by maxima in isopycnal slopes and zonal flow, together with visual inspection of relevant hydrographic property gradients (Orsi et al., 1995). Red line at the surface indicates the sea-ice extent, defined by sea-ice concentrations in excess of 15%.

isopycnals, their PV increases as the sheets draw near the surface in the seasonally ice-covered Southern Ocean. There, the high-PV sheets deviate significantly from density surfaces, as would be expected if diabatic or frictional processes were modifying PV locally. Thus, the structure of the high-PV sheets making up the Southern Hemisphere's internal pycnocline suggests that the elevated stratification is generated in the upper layers of the seasonally ice-covered Southern Ocean. The generation mechanism of the high-PV sheets is assessed next.

3.2. High-PV Generation in the Ice-Covered Southern Ocean

The generation of high PV in the ice-covered Southern Ocean may be understood in terms of two factors. First, the high-PV sheets originate near the surface in areas where salinity overwhelms temperature in determining stratification. This indicates that surface freshwater forcing is likely to play a central role in the creation of the high-PV sheets. Second, in order for these sheets to establish the internal pycnocline, their stratification must survive PV destruction by surface buoyancy loss and vertical mixing in winter.

To further unravel these factors, the seasonal evolution of upper-ocean PV and salinity along a representative meridional section at 100°W, in the Pacific basin, is shown in Figure 2. Panels in each column correspond to every third month of the year, starting in December. Colored contours denote density surfaces of particular significance to the pycnocline's structure, as highlighted in Figure 1. The dashed cyan line marks the mixed layer base. The bottom panels provide the equivalent sections of potential temperature (Figure 2i) and the SCI (Figure 2j) in winter (shown for the month of September). The SCI is an index that indicates the relative contributions of temperature and salinity to setting the stratification, or PV. By construction, the SCI has three distinct regimes: SCI < -1 corresponds to a stable stratification controlled by salinity where the thermal stratification is unstable (as often found in polar regions); $-1 <$ SCI < 1 is associated with thermal and haline stratification that are both stable; and SCI > 1 is obtained when temperature controls the density stratification in the presence of a destabilizing effect of salinity. See Appendix B for a more lengthy explanation of the SCI, and how it relates to other stratification indicators more commonly used in the literature.

The highest PV values occur at the base of the buoyant mixed layer at the end of summer (Figure 2c), when inputs of ice melt, meteoric freshwater and heat create fresh and light Antarctic Surface Water (Figure 2d). The summer mixed layer base marks the location of the seasonal pycnocline (Carmack, 2007; Pellichero et al., 2017). As the atmosphere cools and sea ice (shown by orange bars) rapidly expands in autumn, heat loss and brine rejection deepen the mixed layer and progressively erode the seasonal pycnocline (Figures 2e and 2f). The upper-ocean density increase and mixed layer deepening continue over winter (Figures 2g and 2h). Yet, despite the strong surface buoyancy loss and vertical mixing in autumn and winter, two distinct regions withstand the destruction of high PV at the base of the mixed layer. The 69–72°S latitude band holds the key to the generation and preservation of high PV along the 27.5 kg m^{-3} isopycnal (i.e. the denser of the high-PV sheets making up the internal pycnocline), which reaches its shallowest point and highest PV there. The 63–69°S latitude band hosts the formation of the lighter (27.15 kg m^{-3}) of the high-PV sheets, which attains its maximum PV in the area. Both of these high-PV source regions are characterized by a SCI < -1 (Figure 2j): cold near-surface waters overlie warmer deeper waters in winter, and salinity determines upper-ocean stratification (Figure 2i).

The preferential imprinting of high PV on shallow isopycnals in the two highlighted regions invites us to ask the question of what sets these areas apart. A first step toward an answer is provided by examination of the sea ice-ocean freshwater flux (Figure 3e; the total surface freshwater flux, including surface restoring terms, is shown in Figure C1 and discussed in Appendix C). Both high-PV generation regions host net sea-ice melt in winter. This counter-intuitive result has a different physical explanation in the southern and northern regions. In the southern area (69–72°S), net sea-ice melt is related to upwelling of warm CDW (Wilson et al., 2019), which is shallowest in this region (Figure 2i). Once the seasonal pycnocline has been eliminated in the autumn, sea-ice formation leads to entrainment of warm CDW into the surface mixed layer. The entrained heat melts the existing sea ice and hinders further ice formation (Libera et al., 2022). This well-documented negative feedback on sea-ice formation (Martinson, 1990; Wilson et al., 2019) maintains the low salinity of the mixed layer. As a result, the strong, salinity-determined stratification (i.e. high PV) at the mixed layer base is preserved through winter (Figures 2g and 2j) against the upwelling of CDW (Evans et al., 2018). Thus, the isopycnal lying at the mixed layer base in the area (27.5 kg m^{-3}) is imprinted with high PV.

In contrast, north of 69°S in Figure 2, the sub-surface heat reservoir of CDW lies considerably deeper (Figure 2i) and no longer provides a leading-order feedback on the wintertime evolution of sea ice (Wilson et al., 2019). In this area, high-PV values below the mixed layer are maintained by the continuous influx of sea ice, which drifts from the main freezing sites near the Antarctic margins toward the open ocean (Haumann et al., 2016). The import of sea ice impedes wintertime PV destruction through two effects. First, the sea-ice cover acts as a thermodynamic and mechanical insulator that dampens oceanic heat loss and wind-driven mechanical mixing (Sturm & Massom, 2009; Thorndike & Colony, 1982), and thus suppresses the erosion of upper-ocean stratification. Second, near and to the north of the winter sea-ice edge, near-surface waters remain sufficiently warm year-round to melt sea ice drifting into the region (Figure 3b). Because of these two factors, sea-ice melting prevails over much of the open Southern Ocean—including in winter (Figure 3e)—and the seasonal densification of the mixed layer is limited (Figures 2d–2h). Hence, like in the southern high-PV source region, the surface mixed layer in this area remains very fresh in winter (Figure 2h), despite forcing by the cold and windy atmosphere and by diffusive salt gain from the underlying CDW. Elevated, salinity-determined stratification is then maintained year-round on the isopycnal lying at the base of the winter mixed layer (27.15 kg m^{-3}) in the area straddling the late winter sea-ice edge, and the internal pycnocline's lighter high-PV sheet is formed.

To more quantitatively elicit the separate roles of temperature, salinity and wind forcing on the generation of the subpolar Southern Ocean pycnocline, we now turn to the one-dimensional model for the upper water column introduced in Section 2.2. These one-dimensional simulations are run for two locations along the 100°W Pacific section, at 70°S and 65°S. The temperature and salinity at the surface and at 500 m are restored to values from the global simulations, and the wind forcing is taken from the global model as well. A resulting 3-year time series of $\log_{10}(|PV|)$, shown in Figures 4a and 4b, approximately reproduces the pycnocline's seasonal evolution in the realistic global model. For each of the two Pacific sector locations, we next run three additional 1-d simulations in which we exclude either temperature, salinity or wind forcing at the surface. If we exclude temperature forcing (Figures 4c and 4d), the ensuing pycnocline is very similar to that in the simulation with full forcing, with PV values slightly smaller. If we exclude salinity forcing (Figures 4e and 4f), the pycnocline vanishes and full-depth mixing occurs. If we exclude wind forcing (Figures 4g and 4h), the internal pycnocline is slightly shallower, but still very similar, to that in the simulation with full forcing. These results thus show that it is surface freshwater

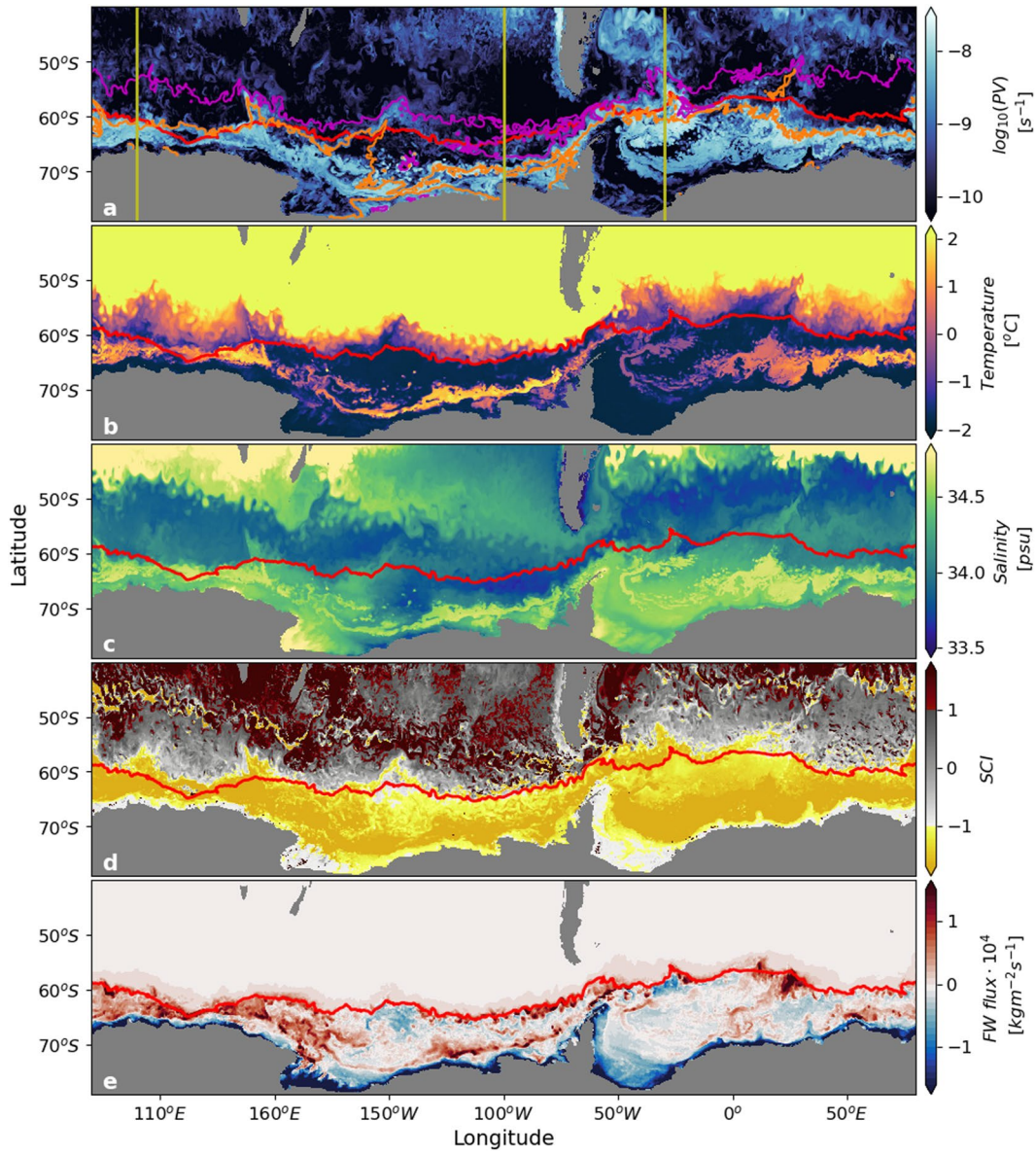

Figure 3. Circumpolar view of pycnocline formation in the upper ocean. (a) $\log_{10}(|PV|)$, (b) temperature, (c) salinity, and (d) Stratification Control Index, at a depth of 89 m in September 2015. (e) Wintertime (July–September 2015) mean of surface freshwater flux due to sea-ice melting and freezing. Positive fluxes are directed into the ocean (melting ice). Magenta and orange contours in panel a respectively indicate isopycnal surfaces $\sigma_\Theta = 27.15$ kg m^{-3} and $\sigma_\Theta = 27.5$ kg m^{-3}. The red line at the surface shows the sea-ice extent, defined as the northern terminus of sea-ice concentrations in excess of 15%. Olive lines in (a) shows the location of the vertical sections shown in Figures 2, 5, and 6.

forcing that is key to generating the internal pycnocline at these locations. Given that almost all surface freshwater forcing in the seasonally ice-covered Southern Ocean is associated with sea ice-ocean interactions (Appendix C, Figure C1), it is evident that only such interactions can generate the internal pycnocline in the beta ocean regime of the Southern Ocean.

To the north of their formation sites, the internal pycnocline's two high-PV sheets descend into the ocean interior along isopycnals at distinct locations (Figure 2). These locations correspond with specific fronts of the Antarctic Circumpolar Current (ACC) (Orsi et al., 1995), where (sub-)mesoscale processes linked to the fronts' enhanced horizontal density gradients and vertical shears have been shown to induce along-isopycnal subduction of near-surface waters (Bachman & Klocker, 2020; Klocker, 2018; A. Naveira Garabato et al., 2001). Examination of Figure 2 indicates that the deeper of the high-PV sheets, extending along the 27.5 kg m^{-3} isopycnal in

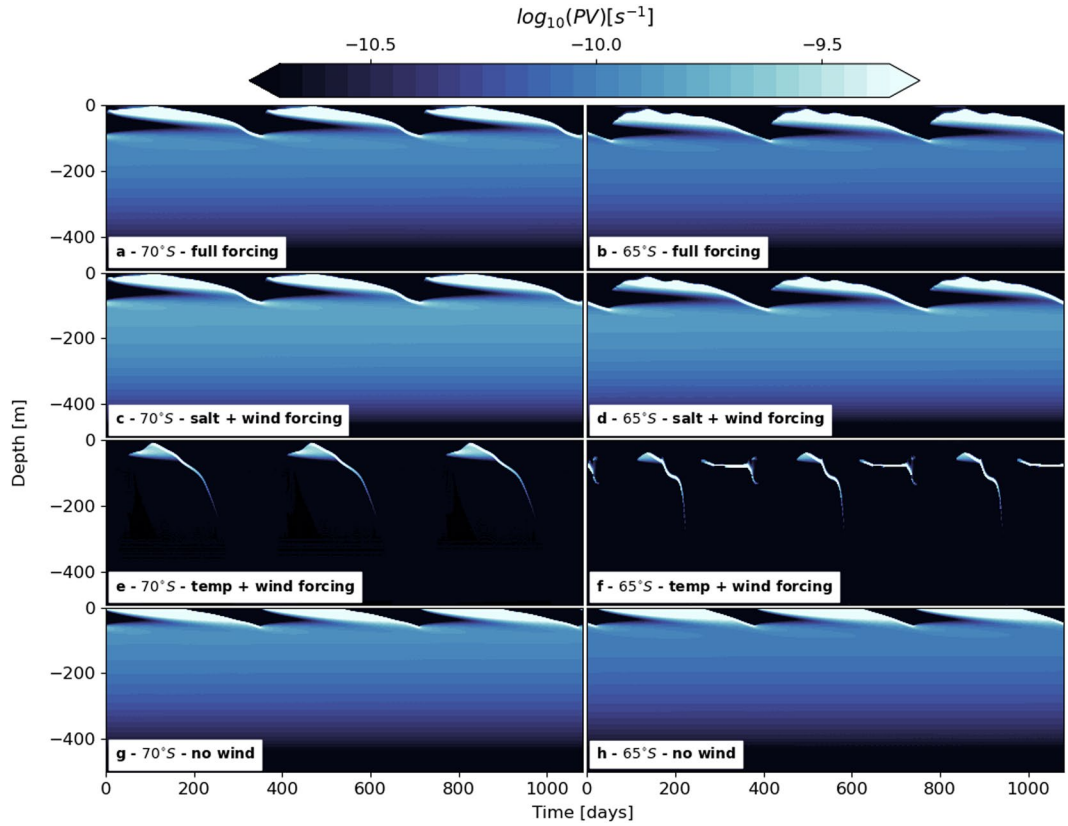

Figure 4. One-dimensional model of pycnocline generation. The evolution of $\log_{10}(|PV|)$ in the one-dimensional model is shown for 3 years, with forcing repeating annually and starting in December 2014, for two Pacific sector locations, (a, c, e, g) 70°S, 100°W and (b, d, f, h) 65°S, 100°W. The simulations are run with (a), (b) the full temperature/salinity/wind forcing, (c), (d) salinity and wind forcing, (e), (f) temperature and wind forcing, and (g), (h) temperature and salinity forcing.

the Pacific basin, departs from the winter mixed layer base and dives into the interior at the Southern ACC Front (SACCF). Similarly, the shallower of the high-PV sheets, found at the 27.15 kg m^{-3} isopycnal in the Pacific sector, descends into the interior at the Polar Front (PF). These qualitative relationships between the spatial configuration of high-PV sheets and the ACC's frontal structure are reproduced all around the Southern Ocean (Figures 2, 5, and 6), and point to the existence of a dynamical underpinning of the sheets' downward and northward continuation from their subpolar generation areas. While the precise nature of these dynamics cannot be ascertained with the model data available, we hypothesize that the descent of the high-PV sheets into the interior is controlled by the same processes that govern frontal subduction (A. Naveira Garabato et al., 2001). Establishing whether this control is exerted directly via the northward transport of elevated PV along the pycnocline's isopycnals, or indirectly via the absence of low-PV injection on those isopycnals, will be the subject of a follow-up study.

3.3. Circumpolar View of Internal Pycnocline Generation

The processes generating the internal pycnocline in the Pacific sector (Figure 2) are widely generic around the Southern Ocean. To illustrate this point, Figures 3a–3d compare the horizontal distributions of wintertime (shown for the month of September) upper-ocean PV, thermohaline properties and SCI at an illustrative depth of 89 m, which is close to the base of the winter mixed layer south of the PF (Figure 2). The wintertime surface freshwater flux due to the melting and freezing of sea ice is also shown in Figure 3e.

Wintertime upper-ocean PV is elevated along a several hundred kilometer-wide, circumpolar swath immediately to the north of the Antarctic continental shelf break (light blue shading in Figure 3a). This swath delineates the generation area of the denser high-PV sheet, as can be gleaned from the approximate spatial correspondence between the band of increased PV and the 27.5 kg m^{-3} isopycnal (orange contour in Figure 3a), on which that high-PV sheet lies in the Pacific basin. The lighter high-PV sheet, formed further to the north, is not visible in

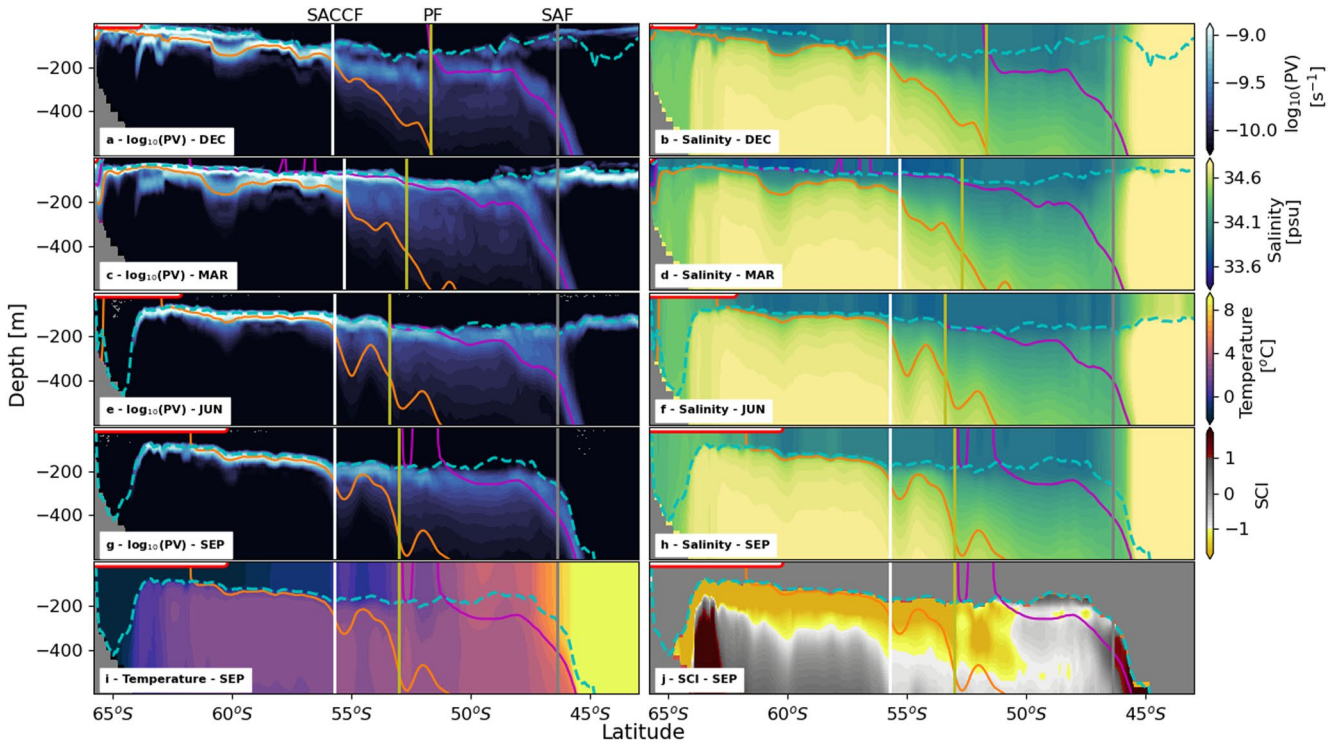

Figure 5. Seasonal evolution of potential vorticity and salinity in the Indian sector. A latitude-depth section at 100°E of (a, c, e, g) $\log_{10}(|PV|)$ and (b, d, f, h) salinity for (a), (b) December, (c), (d) March, (e), (f) June, and (g), (h) September of year 2014/2015. (i) Temperature, and (j) SCI at 100°E for September 2015. Colored dashed lines are isopycnal surfaces $\sigma_\Theta = 27.05$ kg m^{-3} (magenta) and 27.5 kg m^{-3} (orange). Dashed cyan line shows the mixed layer depth. Vertical lines mark Southern Ocean fronts, in particular the Southern ACC front (white), the Polar Front (olive), and the Subantarctic Front (gray). Fronts are identified by maxima in isopycnal slopes and zonal flow, together with visual inspection of relevant hydrographic property gradients (Orsi et al., 1995). Red line at the surface indicates the sea-ice extent, defined by sea-ice concentrations in excess of 15%.

this map because the mixed layer is deeper further north, hence the lighter PV sheet is generated at a greater depth (see the high-PV sheet on the green isopycnal in Figure 2g). The swath of elevated PV encircling Antarctica coincides with an area of higher temperature (Figure 3b) and salinity (Figure 3c), and reduced SCI (SCI < -1, yellow shading in Figure 3d). These indicate the shoaling of relatively warm and saline CDW beneath cold and fresh near-surface waters, which gives rise to strong, salinity-determined upper-ocean stratification. The association of high-PV generation, CDW shoaling and elevated salinity-induced stratification with the ice-ocean feedback outlined above (Martinson, 1990; Wilson et al., 2019) is supported by the horizontal distribution of the surface freshwater flux due to the melting and freezing of sea ice (Figure 3e): the swath of high PV is broadly aligned with a band of substantial freshwater input to the ocean (red shading) fringing the Antarctic continental shelf break.

A second region of enhanced surface freshwater input occurs further to the north, around the winter sea-ice edge (Figure 3e), and is linked to the generation of the lighter high-PV sheet. The excess freshwater forcing in this area produces an abrupt northward reduction in mixed layer salinity (Figure 3c), and is associated with a meridional transition from near-freezing to above-zero mixed layer temperature (Figure 3b). Such thermohaline signatures suggest that the reduction in salinity stems at least in part from the melting of sea ice transported into warmer surface waters via wind-driven, northward Ekman drift (Haumann et al., 2016). More generally, persistent surface freshwater gain in this circumpolar band of reduced surface salinity enables the preservation of elevated PV at the winter mixed layer base on the isopycnal coincident with the lighter high-PV sheet.

Although the key pycnocline formation features highlighted above are quasi-circumpolar, some differences between distinct sectors of the Southern Ocean are also apparent (cf. Figures 2, 5, and 6). Most notably, the South Atlantic internal pycnocline incorporates one high-PV sheet only, at a considerably lighter isopycnal than the denser high-PV sheets in the Indo-Pacific sector. This is because, upon entering the South Atlantic, the ACC veers sharply northward, leading to a significant rearrangement of ACC frontal locations and surface buoyancy

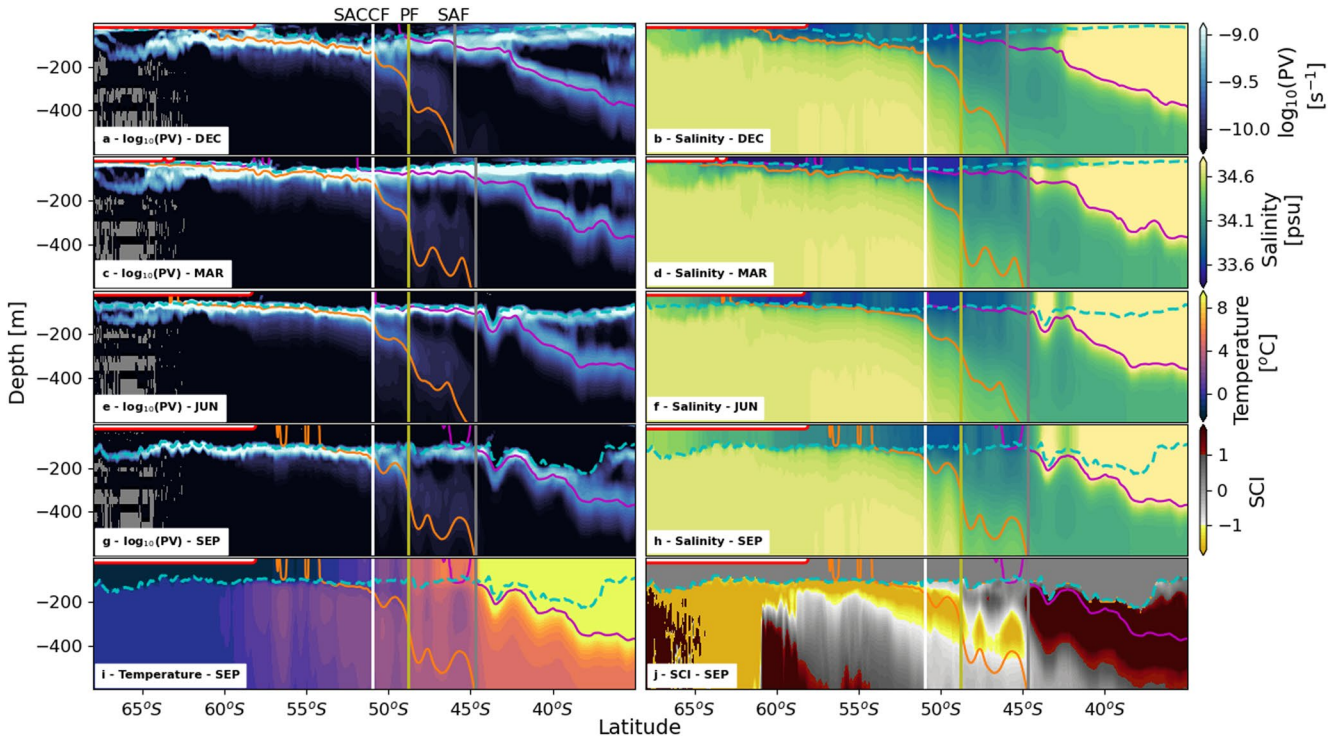

Figure 6. Seasonal evolution of potential vorticity and salinity in the Atlantic sector. A latitude-depth section at 30°W of (a, c, e, g) $\log_{10}(|PV|)$ and (b, d, f, h) salinity for (a), (b) December, (c), (d) March, (e), (f) June, and (g), (h) September of year 2014/2015. (i) Temperature, and (j) SCI at 30°W for September 2015. Colored dash-dotted lines are isopycnal surfaces $\sigma_\Theta = 27.15$ kg m^{-3} (magenta) and 27.5 kg m^{-3} (orange). Dashed cyan line shows the mixed layer depth. Vertical lines mark Southern Ocean fronts, in particular the Southern ACC front (white), the Polar Front (olive), and the Subantarctic Front (gray). Fronts are identified by maxima in isopycnal slopes and zonal flow, together with visual inspection of relevant hydrographic property gradients (Orsi et al., 1995). Red line at the surface indicates the sea-ice extent, defined by sea-ice concentrations in excess of 15%.

flux patterns. As a result, unlike in the other basins, the SACCF in the South Atlantic lies consistently to the north of the winter sea-ice edge, such that all melt-generated, high-PV waters at the winter mixed layer base within this sector are collated into a single sheet descending into the interior at the SACCF (Figure 6).

4. Conclusions and Outlook

Our analysis of a realistic sea ice–ocean model suggests that the internal pycnocline of the high-latitude Southern Ocean is generated by forcing and processes that are distinct from those highlighted by classical views of pycnocline formation (Huang, 1988; Luyten et al., 1983; Robinson & Stommel, 1959; Salmon, 1990; Stommel & Webster, 1962; Welander, 1959; Young & Ierley, 1986), in the following ways.

First, the high stratification defining the internal pycnocline in this region is determined by salinity, whereas classical theories of pycnocline generation focus on oceanic regions with temperature-determined stratification. The stratification control by salinity is primarily a result of the reduced thermal expansion coefficient near the freezing point (Roquet et al., 2022). The key external forcing driving the formation of the region's internal pycnocline is freshwater input by sea-ice melt in winter (Figure 3e). The melting is localized to two distinct zones: one offshore of the Antarctic continental shelf break, where sea-ice melt is sustained by the upward entrainment of warm CDW (Martinson, 1990; Wilson et al., 2019), and another fringing the winter sea-ice edge, where sea ice melts as it drifts northward into warmer surface waters (Haumann et al., 2016). These two wintertime melting zones give rise to two sheets of high stratification, and confer the simulated internal pycnocline with a double stratification-maximum structure (Figure 1). This highlights how the strong coupling between thermal and freshwater forcings associated with sea-ice formation and melt acts to configure ocean stratification on basin scales.

Second, the production of high stratification within the region's internal pycnocline does not stem from the downward projection of a meridional surface density gradient along outcropping isopycnals, as in classical theories

(Luyten et al., 1983; Samelson & Vallis, 1997), but rather from the production of a vertical density gradient at the base of the winter mixed layer. Thus, the density classes hosting the internal pycnocline across and beyond the high-latitude Southern Ocean need not reach the surface to acquire their elevated stratification. This implies that the internal pycnocline's density structure may be controlled by sub-surface mixing processes around the mixed layer base, rather than directly by buoyancy fluxes across the ocean surface.

Third, our finding that the descent of the high-PV sheets into the ocean interior is localized to specific ACC fronts suggests that (sub-)mesoscale upper-ocean frontal dynamics may shape this stage of pycnocline formation. This contrasts with classical views, which rationalize the downward projection of the pycnocline in terms of large-scale, wind-driven Ekman flows and, in some cases, the integrated effects of deep baroclinic eddies (Nikurashin & Vallis, 2012; Wolfe & Cessi, 2010).

In conclusion, elevated stratification within the high-latitude Southern Ocean internal pycnocline is generated by winter-persistent sea ice melting, and descends into the ocean interior at ACC fronts. Both of these elements are absent from current theoretical perspectives on pycnocline formation, including those considering the Southern Ocean's role (Gnanadesikan, 1999; Karsten et al., 2002; D. P. Marshall et al., 2017; Nikurashin & Vallis, 2012; Wolfe & Cessi, 2010). Such Southern Ocean-focused theories imply that the internal pycnocline's depth is determined by an intricate interplay between wind forcing, baroclinic eddies and surface buoyancy fluxes. However, they assume that the internal pycnocline's stratification reflects the meridional density gradient at the surface of the Southern Ocean, and that this gradient is shaped by annual-mean surface buoyancy fluxes. Our work indicates that establishment of the internal pycnocline relies on the maintenance of a strong vertical density gradient at the base of the winter mixed layer in subpolar seas, enabled by the northward drift of Antarctic sea ice and the persistence of net sea ice melt.

A pressing question emerging from this work concerns how the internal pycnocline generation mechanism discussed here, which focuses on the Southern Ocean's beta ocean regime, connects to classical pycnocline theories applying to the alpha ocean regime equatorward of the Southern Ocean. The illustrations of the internal pycnocline's structure in Figure 1 shows that the pycnocline transitions smoothly across the alpha-beta ocean boundary. This points to the existence of a link between global-ocean transport pathways (such as the overturning circulation) and sea-ice ocean interactions in the Southern Ocean—the nature of which is difficult to untangle from the available monthly mean model output considered in our study. One possibility is that the internal pycnocline is primarily generated in the subpolar Southern Ocean as explained in this work, and that the pycnocline's high-PV sheets are then projected northward by for example, mesoscale eddy stirring. Another possibility is that the internal pycnocline in the alpha ocean regime to the north of the Southern Ocean is generated as proposed by classical theories, and that there is a long-timescale adjustment between the processes governing northern and Southern Ocean pycnocline formations—such that a continuous internal pycnocline emerges across the alpha-beta ocean transition.

The main caveat of this work is that much of the analysis is qualitative. The large computational resources required for these model simulations limit our ability to run multiple sensitivity experiments, and to save the model output needed to perform a more quantitative analysis. A further challenge to more quantitatively test the ideas put forward here is the wide range of spatio-temporal scales of the processes pertinent to internal pycnocline formation. Such scales span from the subdaily timescales of the localized turbulent processes implicated in entrainment to the centennial (and longer) timescales of basin-wide adjustment equatorward of the Southern Ocean. Thus, elucidating the role of ice-ocean interactions in the Southern Ocean in generating the internal pycnocline is likely to require a dual approach that captures and connects such disparate scales. Process-targeted observations and turbulence-resolving modeling of the evolution of Southern Ocean stratification under ice will be required to unravel the key stratification-controlling processes. In turn, a hierarchy of basin-scale, eddy-resolving models of varying degree of idealization will be needed to establish the mechanisms via which under-ice Southern Ocean processes may influence, or be influenced by, the rest of the global ocean. While these requirements pose major technological and computational difficulties, the recent rapid changes exhibited by Southern Ocean sea ice (Eayrs et al., 2021) highlight the importance of discerning the potential pycnocline-generating role of regional ice-ocean interactions.

Appendix A: Model Comparison With Observations

While the model is thoroughly validated elsewhere (Kiss et al., 2020), for the purpose of this work we note that the model broadly reproduces the observed structure of the internal pycnocline (cf. Figures 1 and A1),

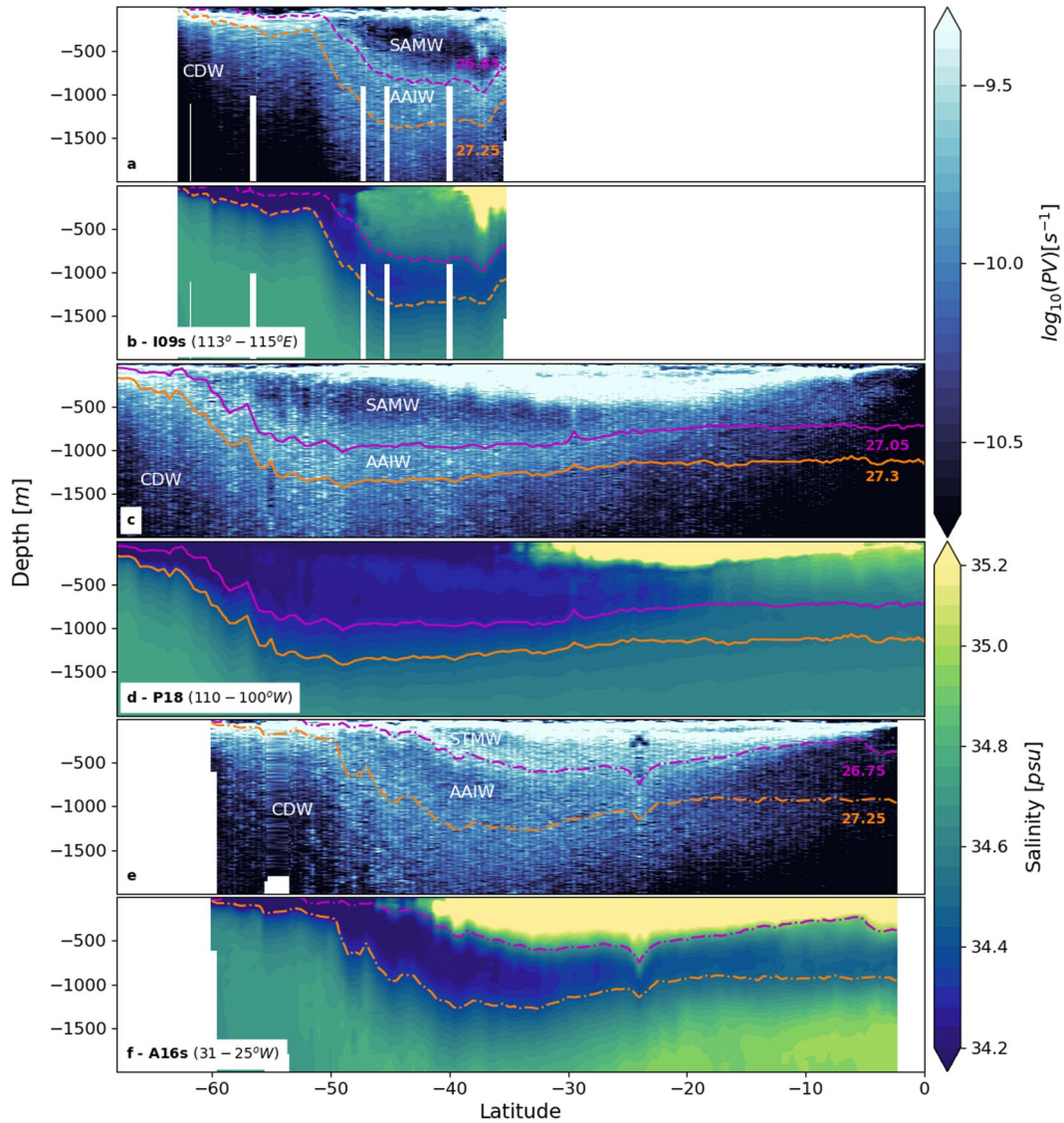

Figure A1. Potential vorticity and salinity from observations. Ship-based observations of (a, c, e) $\log_{10}(|PV|)$ and (b, d, f) salinity. (a), (b) WOCE transect I09s from a R/V Aurora Australis cruise in January–February 2012, (c), (d) WOCE transect P18 from a R/V Ronald H. Brown cruise in November 2016–February 2017, and (e), (f) WOCE transect A16s from R/V Ronald H. Brown cruise in January–February 2005. Colored lines are isopycnal surfaces approximately associated with the upper (magenta) and lower (orange) high-PV sheets, which together form the internal pycnocline. Subtropical Mode Water (STMW), Subantarctic Mode Water (SAMW), Antarctic Intermediate Water (AAIW), and Circumpolar Deep Water (CDW) are labeled.

with two modest differences. First, the separation between high-stratification sheets in the observations is more subtle than in the model. This is at least in part due to observations, which represent a snapshot of the ocean, also including finescale motions (e.g., internal waves) and measurement noise. It is also likely that the model exaggerates the inter-sheet gap in the ocean interior, as the model's limited resolution does not fully capture the (sub-)mesoscale re-stratification processes expected to moderate vertical gradients in interior stratification (Bachman & Klocker, 2020), and as the model includes no background vertical diffusivity. Second, the densities of the observed high-stratification sheets are slightly lighter (typically by 0.1–0.2 kg m^{-3}) than those in the model.

Appendix B: Stratification Control Index

A key theoretical concept in our analysis of the model simulation is the Stratification Control Index, SCI, which is considered here to assess the degree of spiciness in a stable stratification (Stewart & Haine, 2016). The SCI is defined as the ratio of the spice frequency, $K^2 = g(\alpha\partial_z\Theta + \beta\partial_z S_A)$, to the buoyancy frequency, $N^2 = g(\alpha\partial_z\Theta - \beta\partial_z S_A)$, where g is the gravitational acceleration, α is the thermal expansion coefficient, and β is the haline contraction coefficient (Ioc & Iapso, 2010). Since planetary PV is proportional to the stratification, SCI can equally be interpreted to indicate the relative contributions of temperature and salinity to setting PV. By construction, the SCI has three distinct regimes: SCI < -1 corresponds to a stable stratification controlled by salinity where the thermal stratification is unstable (as often found in polar regions); $-1 <$ SCI < 1 is associated with thermal and haline stratifications that are both stable; and SCI > 1 is obtained when temperature controls the density stratification in the presence of a destabilizing effect of salinity.

The SCI can be connected to several other stratification indicators more commonly used in the literature. The density ratio, $R_\sigma = (\alpha\partial_z\Theta)/(\beta\partial_z S_A)$, was first introduced by Turner (1973) and can be related to the SCI as $R_\sigma = (\text{SCI} + 1)(\text{SCI} - 1)$. A difficulty with the density ratio is that it diverges when the salinity stratification vanishes, even in the presence of a stable thermal stratification. This is the reason why the SCI is preferred here. Subsequently, the Turner angle was also determined as the arc tangent of the ratio of spice to buoyancy frequencies (Ruddick, 1983). Hence, the SCI is simply the tangent of the Turner angle, uniquely defined for any stable stratification. Drawing on the properties of the Turner angle, salt fingering is implied to occur when SCI > 1, and diffusive convection develops when SCI < -1.

Appendix C: Thermal and Haline Surface Buoyancy Fluxes

The surface buoyancy flux, B, depends on both surface heating and freshwater input, and can be expressed as (Cronin & Sprintall, 2001)

$$B = \underbrace{-\frac{g\alpha Q}{\rho c_p}}_{B_H} + \underbrace{g\beta F_w SSS}_{B_{FW}}, \tag{C1}$$

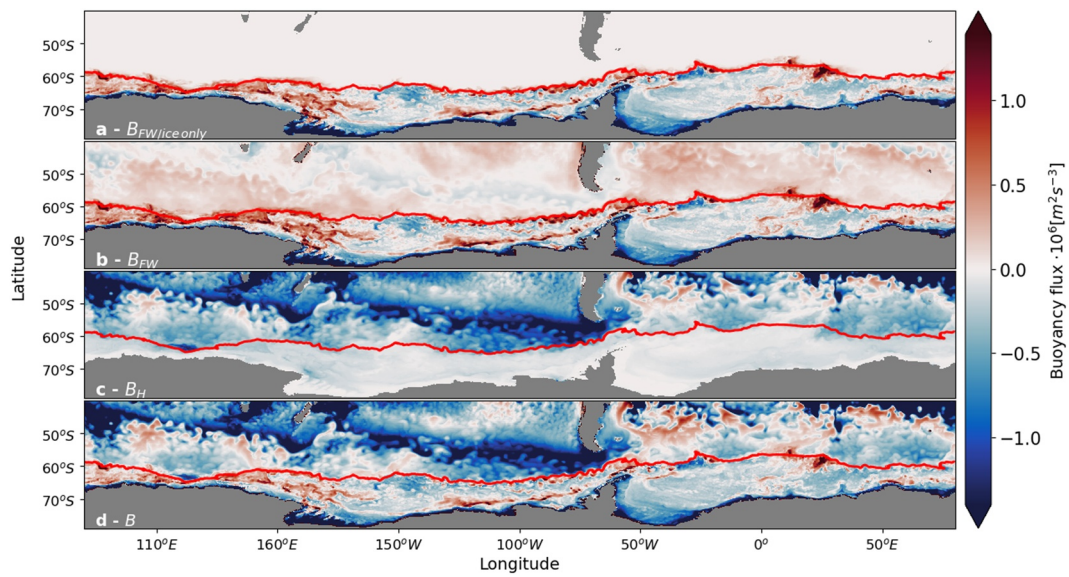

Figure C1. Surface buoyancy flux in the Southern Ocean. Wintertime (mean over July–September 2015) surface buoyancy flux due to (a) freshwater from sea-ice melting and freezing, (b) total surface freshwater input, and (c) surface heat flux. (d) Net surface buoyancy flux. Positive fluxes are directed into the ocean. The red line shows the sea-ice extent, defined as the northern terminus of sea-ice concentrations in excess of 15%.

where B_H is the buoyancy flux due to heating and cooling, and B_{FW} is the buoyancy flux due to freshwater input or loss. Q is the surface heat flux, F_w the surface freshwater input, ρ the surface density, c_p the specific heat capacity of seawater, and SSS the sea surface salinity. Q has units of W m^{-2}, F_w has units of m s^{-1}, and B has units of m^2 s^{-3}. In the coupled sea ice-ocean model used here, surface ocean fluxes are due to (a) restoring toward observed SSS, (b) heat and freshwater exchanges with the atmosphere deduced from bulk formulas and the JRA55-do v1.3 forcing data set, and (c) freshwater fluxes resulting from the melting and freezing of sea ice. In winter (Figure C1, showing a mean over July–September 2015), the surface buoyancy flux indicates that changes in upper-ocean buoyancy under sea ice are almost entirely due to freshwater fluxes induced by the melting and freezing of sea ice. North of the sea-ice edge, the surface buoyancy flux transitions to being largely dominated by surface heat fluxes.

Data Availability Statement

All the data used in this work are publicly available. The model code is available at github.com/COSIMA/access-om2, and the model output can be accessed at http://dx.doi.org/10.4225/41/5a2dc8543105a. Observational transects can be downloaded at https://cchdo.ucsd.edu/cruise/09AR20120105 (WOCEtransect I09s), https://cchdo.ucsd.edu/cruise/33RO20161119 (WOCE transect P18), and https://cchdo.ucsd.edu/cruise/33RO200501 (WOCE transect A16s).

Acknowledgments
The authors thank the Consortium for Ocean-Sea Ice Modeling in Australia (COSIMA; www.cosima.org.au) for making the ACCESS-OM2 suite of models available at github.com/COSIMA/access-om2. Model runs were undertaken with the assistance of resources from the National Computational Infrastructure (NCI), which is supported by the Australian Government. This research was supported under Australian Research Council's Special Research Initiative for Antarctic Gateway Partnership (Project ID SR140300001). This project received grant funding from the Australian Government as part of the Antarctic Science Collaboration Initiative program. The work was supported in part by the Centre for Southern Hemisphere Oceans Research, a partnership between CSIRO, the Qingdao National Laboratory for Marine Science and Technology, the University of New South Wales and the University of Tasmania and by the Australian Antarctic Program Partnership.

References

Bachman, S., & Klocker, A. (2020). Interaction of jets and submesoscale dynamics leads to rapid ocean ventilation. *Journal of Physical Oceanography*, *50*(10), 2873–2883. https://doi.org/10.1175/JPO-D-20-0117.1

Bullister, J. L., Rhein, M., & Mauritzen, C. (2001). Deepwater Formation. In G. Siedler, S. M. Griffies, J. Gould, & J. A. Church (Eds.), *Ocean circulation and climate: A 21st century perspective* (pp. 227–253). Academic Press.

Carmack, E. C. (2007). The alpha/beta ocean distinction: A perspective on freshwater fluxes, convection, nutrients and productivity in high-latitude seas. *Deep-Sea Research Part II Topical Studies in Oceanography*, *54*(23–26), 2578–2598. https://doi.org/10.1016/j.dsr2.2007.08.018

Cronin, M., & Sprintall, J. (2001). Wind and buoyancy-forced upper ocean. In *Encyclopedia of ocean sciences* (pp. 3219–3226). Elsevier. https://doi.org/10.1006/rwos.2001.0157

DeVries, T., & Primeau, F. (2011). Dynamically and observationally constrained estimates of water-mass distributions and ages in the global ocean. *Journal of Physical Oceanography*, *41*(12), 2381–2401. https://doi.org/10.1175/JPO-D-10-05011.1

Eayrs, C., Li, X., Raphael, M. N., & Holland, D. M. (2021). Rapid decline in Antarctic sea ice in recent years hints at future change. *Nature Geoscience*, *14*(7), 460–464. https://doi.org/10.1038/s41561-021-00768-3

Evans, D. G., Zika, J. D., Naveira Garabato, A. C., & Nurser, A. J. (2018). The cold transit of Southern Ocean upwelling. *Geophysical Research Letters*, *45*(24), 13386–13395. https://doi.org/10.1029/2018GL079986

Gnanadesikan, A. (1999). A simple predictive model for the structure of the oceanic pycnocline. *Science*, *283*(5410), 2077–2079. https://doi.org/10.1126/science.283.5410.2077

Haumann, F. A., Gruber, N., Münnich, M., Frenger, I., & Kern, S. (2016). Sea-ice transport driving Southern Ocean salinity and its recent trends. *Nature*, *537*(7618), 89–92. https://doi.org/10.1038/nature19101

Huang, R. X. (1988). On boundary value problems of the ideal-fluid thermocline. *Journal of Physical Oceanography*, *18*(4), 619–641. https://doi.org/10.1175/1520-0485(1988)018<0619:OBVPOT>2.0.CO;2

Ioc, S., & Iapso (2010). The international thermodynamic equation of seawater – 2010: Calculation and use of thermodynamic properties. *Intergovernmental Oceanographic Commission, Manuals and Guides No.*, *56*, 196.

Karsten, R., Jones, H., & Marshall, J. (2002). The role of eddy transfer in setting the stratification and transport of a circumpolar current. *Journal of Physical Oceanography*, *32*(1), 39–54. https://doi.org/10.1175/1520-0485(2002)032<0039:TROETI>2.0.CO;2

Khatiwala, S., Primeau, F., & Holzer, M. (2012). Ventilation of the deep ocean constrained with tracer observations and implications for radiocarbon estimates of ideal mean age. *Earth and Planetary Science Letters*, *325–326*, 116–125. https://doi.org/10.1016/j.epsl.2012.01.038

Kiss, A., McC Hogg, A., Hannah, N., Boeira Dias, F., Brassington, G. B., Chamberlain, M., et al. (2020). ACCESS-OM2 v1.0: A global ocean-sea ice model at three resolutions. *Geoscientific Model Development*, *13*(2), 401–442. https://doi.org/10.5194/gmd-13-401-2020

Klocker, A. (2018). Opening the window to the Southern Ocean: The role of jet dynamics. *Science Advances*, *4*(10). https://doi.org/10.1126/sciadv.aao4719

Large, W. G., McWilliams, J. C., & Doney, S. C. (1994). Oceanic vertical mixing: A review and a model with a nonlocal boundary layer parameterization. *Reviews of Geophysics*, *32*(4), 363–403. https://doi.org/10.1029/94RG01872

Lecomte, O., Goosse, H., Fichefet, T., De Lavergne, C., Barthélemy, A., & Zunz, V. (2017). Vertical ocean heat redistribution sustaining sea-ice concentration trends in the Ross Sea. *Nature Communications*, *8*(1), 258. https://doi.org/10.1038/s41467-017-00347-4

Libera, S., Hobbs, W., Klocker, A., Meyer, A., & Matear, R. (2022). Ocean-sea ice processes and their role on multi-month predictability of Antarctic Sea ice. *Geophysical Research Letters*, *49*(8), 1–10. https://doi.org/10.1029/2021gl097047

Luyten, J. R., Pedlosky, J., & Stommel, H. (1983). The ventilated thermocline. *Journal of Physical Oceanography*, *13*(2), 292–309. https://doi.org/10.1175/1520-0485(1983)013<0292:TVT>2.0.CO;2

Marshall, D. P., Ambaum, M. H., Maddison, J. R., Munday, D. R., & Novak, L. (2017). Eddy saturation and frictional control of the Antarctic Circumpolar Current. *Geophysical Research Letters*, *44*(1), 286–292. https://doi.org/10.1002/2016GL071702

Marshall, J., Adcroft, A. J., Hill, C., Perelman, L., & Heisey, C. (1997). A finite-volume, incompressible {N}avier {S}tokes model for studies of the ocean on parallel computers. *Journal of Geophysical Research*, *102*(C3), 5753–5766. https://doi.org/10.1029/96jc02775

Marshall, J., Olbers, D., Ross, H., & Wolf-Gladrow, D. (1993). Potential vorticity constraints on the dynamics and hydrography of the Southern Ocean. *Journal of Physical Oceanography*, *23*(3), 465–487. https://doi.org/10.1175/1520-0485(1993)023<0465:PVCOTD>2.0.CO;2

Martinson, D. G. (1990). Evolution of the southern ocean winter mixed layer and sea ice: Open ocean deepwater formation and ventilation. *Journal of Geophysical Research*, *95*(C7), 11641. https://doi.org/10.1029/jc095ic07p11641
McCartney, M. S. (1977). Subantarctic mode water. *Deep-Sea Research*, *24*, 103–119.
Naveira Garabato, A. C., Allen, J., Leach, H., Strass, V., Pollard, R., Garabato, A., & Leach, H. (2001). Mesoscale subduction at the Antarctic Polar Front driven by baroclinic instability. *Journal of Physical Oceanography*, *31*(8), 2087–2107. https://doi.org/10.1175/1520-0485(2001)031<2087:MSATAP>2.0.CO;2
Naveira Garabato, A. C., Williams, A. P., & Bacon, S. (2014). The three-dimensional overturning circulation of the Southern Ocean during the WOCE era. *Progress in Oceanography*, *120*, 41–78. https://doi.org/10.1016/j.pocean.2013.07.018
Nikurashin, M., & Vallis, G. (2012). A theory of the interhemispheric meridional overturning circulation and associated stratification. *Journal of Physical Oceanography*, *42*(10), 1652–1667. https://doi.org/10.1175/JPO-D-11-0189.1
Nycander, J., Hieronymus, M., & Roquet, F. (2015). The nonlinear equation of state of sea water and the global water mass distribution. *Geophysical Research Letters*, *42*(18), 7714–7721. https://doi.org/10.1002/2015GL065525
Orsi, A. H., Whitworth, T., & Nowlin, W. D. (1995). On the meridional extent and fronts of the Antarctic Circumpolar Current. *Deep-Sea Research Part I*, *42*(5), 641–673. https://doi.org/10.1016/0967-0637(95)00021-W
Pellichero, V., Sallée, J.-B., Schmidtko, S., Roquet, F., & Charrassin, J.-B. (2017). The ocean mixed layer under Southern Ocean sea-ice: Seasonal cycle and forcing. *Journal of Geophysical Research: Oceans*, *122*(2), 1608–1633. https://doi.org/10.1002/2016JC011970
Polyakov, I. V., Pnyushkov, A. V., Alkire, M. B., Ashik, I. M., Baumann, T. M., Carmack, E. C., et al. (2017). Greater role for Atlantic inflows on sea-ice loss in the Eurasian Basin of the Arctic Ocean. *Science*, *356*(6335), 285–291. https://doi.org/10.1126/science.aai8204
Robinson, A., & Stommel, H. (1959). The oceanic thermocline and the associated thermohaline circulation. *Tellus*, *11*(3), 295–308. https://doi.org/10.3402/tellusa.v11i3.9317
Roquet, F., Ferreira, D., Caneill, R., Schlesinger, D., & Madec, G. (2022). Unique thermal expansion properties of water key to the formation of sea ice on Earth. *Science Advances*, *8*(46), eabq0793. https://doi.org/10.1126/sciadv.abq0793
Roquet, F., Madec, G., Brodeau, L., & Nycander, J. (2015). Defining a simplified yet "Realistic" equation of state for seawater. *Journal of Physical Oceanography*, *45*(10), 2564–2579. https://doi.org/10.1175/JPO-D-15-0080.1
Ruddick, B. (1983). A practical indicator of the stability of the water column to double-diffusive activity. *Deep-Sea Research, Part A: Oceanographic Research Papers*, *30*(10), 1105–1107. https://doi.org/10.1016/0198-0149(83)90063-8
Salmon, R. (1990). The thermocline as an "internal boundary layer". *Journal of Marine Research*, *48*(3), 437–469. https://doi.org/10.1357/002224090784984650
Samelson, R. M., & Vallis, G. K. (1997). Large-scale circulation with small diapycnal diffusion: The two-thermocline limit. *Journal of Marine Research*, *55*(2), 223–275. https://doi.org/10.1357/0022240973224382
Speer, K., & Forget, G. (2001). Global distribution and formation of mode waters. In G. Siedler, S. M. Griffies, J. Gould, & J. A. Church (Eds.), *Ocean circulation and climate: A 21st century perspective* (pp. 211–226). Academic Press.
Stewart, K. D., & Haine, T. W. (2016). Thermobaricity in the transition zones between alpha and beta oceans. *Journal of Physical Oceanography*, *46*(6), 1805–1821. https://doi.org/10.1175/JPO-D-16-0017.1
Stommel, H., & Webster, J. (1962). Some properties of thermocline equations in a subtropical gyre. *Journal of Marine Research*, *20*(1), 42–56.
Sturm, M., & Massom, R. A. (2009). Snow and sea ice. In *Sea ice* (pp. 153–204). Wiley-Blackwell. https://doi.org/10.1002/9781444317145.ch5
Talley, L. D. (2013). Closure of the global overturning circulation through the Indian, Pacific, and southern oceans. *Oceanography*, *26*(1), 80–97. https://doi.org/10.5670/oceanog.2013.07
Talley, L. D., Feely, R. A., Sloyan, B. M., Wanninkhof, R., Baringer, M. O., Bullister, J. L., et al. (2016). Changes in ocean heat, carbon content, and ventilation: A review of the first decade of GO-SHIP global repeat hydrography. *Annual Review of Marine Science*, *8*(1), 185–215. https://doi.org/10.1146/annurev-marine-052915-100829
Tamsitt, V., Drake, H. F., Morrison, A. K., Talley, L. D., Dufour, C. O., Gray, A. R., et al. (2017). Spiraling pathways of global deep waters to the surface of the Southern Ocean. *Nature Communications*, *8*(1), 1–10. https://doi.org/10.1038/s41467-017-00197-0
Thorndike, A. S., & Colony, R. (1982). Sea ice motion in response to geostrophic winds. *Journal of Geophysical Research*, *87*(C8), 5845. https://doi.org/10.1029/jc087ic08p05845
Turner, J. S. (1973). *Buoyancy effects in fluids*. Cambridge University Press. https://doi.org/10.1017/CBO9780511608827
Vallis, G. K. (2006). *Atmospheric and oceanic fluid dynamics*. Cambridge University Press. https://doi.org/10.1017/cbo9780511790447
Welander, P. (1959). An advective model of the ocean thermocline. *Tellus*, *11*(3), 309–318. https://doi.org/10.3402/tellusa.v11i3.9316
Wilson, E. A., Riser, S. C., Campbell, E. C., & Wong, A. P. (2019). Winter upper-ocean stability and ice-ocean feedbacks in the sea ice-covered Southern Ocean. *Journal of Physical Oceanography*, *49*(4), 1099–1117. https://doi.org/10.1175/JPO-D-18-0184.1
Wolfe, C. L., & Cessi, P. (2010). What sets the strength of the middepth stratification and overturning circulation in eddying ocean models? *Journal of Physical Oceanography*, *40*(7), 1520–1538. https://doi.org/10.1175/2010JPO4393.1
Young, W. R., & Ierley, G. R. (1986). Eastern boundary conditions and weak solutions of the ideal thermocline equations. *Journal of Physical Oceanography*, *16*(11), 1884–1900. https://doi.org/10.1175/1520-0485(1986)016<1884:EBCAWS>2.0.CO;2